ACS APPLIED MATERIALS & INTERFACES

LETTER

www.acsami.org

Binder-Free Manganese Oxide/Carbon Nanomaterials Thin Film Electrode for Supercapacitors

Ning Wang, Chuxin Wu, Jiaxin Li, Guofa Dong, and Lunhui Guan*

State Key Laboratory of Structural Chemistry, Fujian Institute of Research on the Structure of Matter, Chinese Academy of Sciences, YangQiao West Road 155#, Fuzhou, Fujian 350002, P. R. China

Supporting Information

ABSTRACT: A ternary thin film electrode was created by coating manganese oxide onto a network composed of single-walled carbon nanotubes and single-walled carbon nanohorns. The electrode exhibited a porous structure, which is a promising architecture for supercapacitors applications. The maximum specific capacitances of 357 F/g for total electrode at 1 A/g were achieved in 0.1 M Na_2SO_4 aqueous solution.

KEYWORDS: MnO_2, SWNT, SWNH, thin film, porous structure, supercapacitors

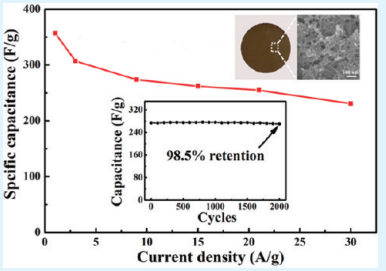

Supercapacitors are very attractive for the high power density and long cycle-life. They could be applied to many fields such as hybrid electric vehicles, portable devices and other renewable energy storage applications.[1−3] Among the various structures of the electrodes for supercapacitors, thin film architecture is attractive because it can reduce the equivalent series resistance of electrodes and shows high power densities.[4,5] An ideal material for thin film electrode must have a highly electrolyte accessible network, high conductivity, and mechanical stability.[6] For instance, carbon nanotubes (CNTs) have been proved to be a prominent candidate for binder free thin film electrodes with good electrochemical performance in nonaqueous electrolytes.[7−9] For thin film electrode based on carbon materials, control of the balanced surface area and mesoporosity is of critical importance to allow the effective permeation of the electrolytes. Recently, the performances of CNT thin film electrodes were further improved by tailoring their pore structure, which is a key role for electrolyte accessibility.[10,11] Meanwhile, the carbon-based thin film electrodes were usually used in nonaqueous electrolytes. They suffered from low capacitance in aqueous electrolytes. To increase the capacitance in aqueous electrolytes, metal oxides that undergo fast surface redox reactions (pseudocapacitance) were introduced into the electrodes.[12−14] It is expected that incorporation of nanosized manganese oxide (MnO_2) into a porous carbon framework could improve the utilization of MnO_2 pseudocapacity and high surface and mesoporosity of the electrode, thus dramatically improve their performance.

So in this study, we first synthesized a porous network composed of single-walled carbon nanotubes (SWNTs) and single-walled carbon nanohorns (SWNHs), then directly coated MnO_2 on them based on the spontaneous redox reaction given in eq 1,[15] eventually to form a ternary nanocomposite for high-performance supercapacitors.

$$4KMnO_4 + 3C + H_2O \rightarrow 4MnO_2 + K_2CO_3 + 2KHCO_3 \quad (1)$$

In the ternary nanocomposites, SWNTs are the fundamental scaffoldings, providing good conductivity and mechanical stability for the electrode. SWNHs tailor the pore structure of SWNT thin film, enable fast access of electrolyte. MnO_2 increases the overall capacitance of electrode. The as-prepared electrodes exhibit a porous structure checked by scanning electron microscopy (SEM) and transmission electron microscopy (TEM). Cyclic voltammetry (CV) and galvanostatic charge/discharge cycling tests demonstrate that the ternary nanocomposites electrodes exhibit an attractive electrochemical performance in neutral aqueous electrolytes.

As illustrated in Scheme 1, MnO_2/SWNH/SWNT electrodes are obtained in three steps. First, a suspension solution of SWNH and SWNT was prepared by sonication. Then the SWNH/SWNT thin films were obtained by a vacuum filtration method and transferred onto indium−tin oxide (ITO) substrates.[16] After heat treatment, the as-obtained thin films on ITO were dipped into a stirred $KMnO_4$ solution to incorporate MnO_2. Without any binder, a stable MnO_2/SWNH/SWNT thin film electrode was prepared. The SWNT and MnO_2/SWNT thin films were created for comparison by the same methods. The mass of coating MnO_2 could be controlled by adjusting the dipping time and determined with an atomic absorption spectrophotometer.[17] The weight ratio of MnO_2 was 30% in the overall electrode when the dipping time was 60 min in this work.

The morphologies of the as-prepared thin films are displayed in the SEM images and shown in Figure 1. Figure 1a shows an interconnected network structure composed of SWNT bundles for the comparison with SWNT thin film. After being dipped in $KMnO_4$ solution, the surface of SWNT thin film is covered fully by generated MnO_2 layer because the pores between SWNT bundles were filled with MnO_2 (Figure 1b). Figure 1c shows the

Received: August 23, 2011
Accepted: October 11, 2011
Published: October 11, 2011

Scheme 1. (a) Diagram of Preparing the MnO_2/SWNH/SWNT Electrode and (b) Corresponding Optical Images

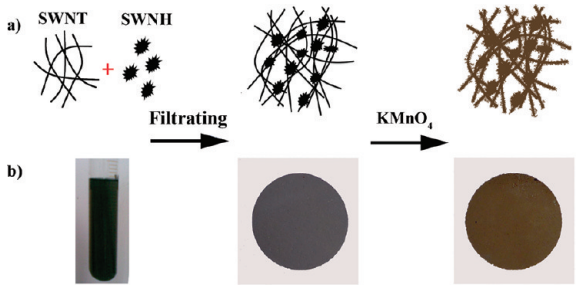

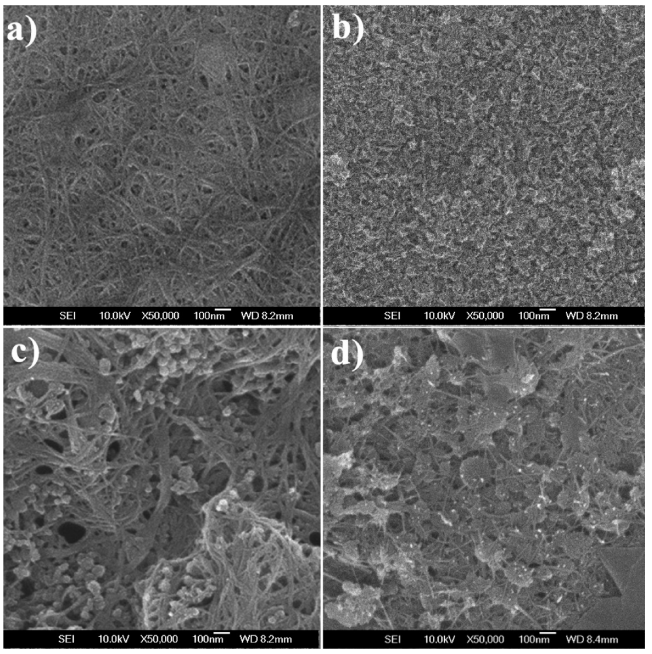

Figure 1. SEM images of the (a) SWNT, (b) MnO_2/SWNT, (c) SWNH/SWNT, and (d) MnO_2/SWNH/SWNT thin films.

microstructure of the SWNH/SWNT thin film, revealing more abundant pore distribution compared with SWNT thin film. Hence, this porous structure ensures larger available surface area than SWNT, agreeing with the result of Brunauer–Emmett–Teller analysis (see Figure S1a in the Supporting Information). The pore size emerged a new distribution centered at ~20 nm (see Figure S1b in the Supporting Information), as a result of the SWNH particles act as a role of spacer which leads to the pore structure.[10] The pores with large size would not be blocked in the generating process of MnO_2, proved by the SEM image of the SWNH/SWNT after dipped in $KMnO_4$ solution. Figure 1d demonstrates the porous structure is still kept although SWNH/SWNT network was coated by MnO_2 layer. This porous structure is necessary for a high-performance electrochemical electrode because it ensures easy electrolyte access to a large volume of active electrode materials, as discussed later.

To investigate the microstructure of as-prepared electrodes, TEM imaging and selected-area electron diffraction (SAED) analysis were employed, as shown in Figure 2. Figure 2a shows the components of the SWNH/SWNT thin film. The white

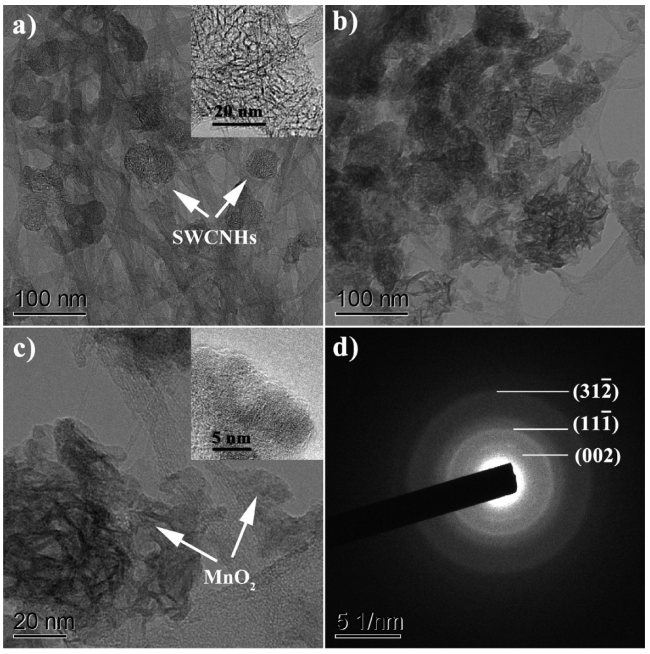

Figure 2. (a) TEM images of the SWNH/SWNT thin film electrode, (b, c) TEM images, and (d) SAED of the MnO_2/SWNH/SWNT thin film electrode.

arrows indicate the SWNHs, which adhere to SWNTs and are interconnected to form a porous structure. The inset in Figure 2a reveals the morphology of SWNH with higher magnification. Figure 2b shows the TEM image of SWNH/SWNT thin film coated by MnO_2 layer. The MnO_2 layer directly grows onto the carbon template based on the spontaneously redox reaction according to the eq 1, which enables the electron to transfer fast between carbon template and MnO_2. Noteworthy, the distributions of MnO_2 are not uniform because of different reaction activities for SWNHs and SWNTs. SWNHs with a conical structure easily react with $KMnO_4$ and are covered fully by MnO_2. SWNTs are only covered partly by MnO_2 layer for their relative inert character compared with SWNHs. This result is further proved by the TEM image with high resolution (Figure 2c). The typical locations of MnO_2 are indicated by the white arrows, demonstrating the nonuniform distributions of MnO_2. The inset of Figure 2c shows the TEM image with higher magnification of MnO_2, which distinguishes MnO_2 from SWNH. Meanwhile, the nonuniform MnO_2 coating leaves more pores within electrode, contributing to the formation of porous structure. The pattern of SAED is shown in Figure 1d. Three rings are observed from the image: the rings correspond to the (31$\bar{2}$), (11$\bar{1}$), and (002) planes of MnO_2. The nonobvious feature of the rings reveals the defect-rich crystallization of MnO_2.

The electrochemical properties of the thin film electrodes were examined by CV and galvanostatic charge/discharge tests. Figure 3a shows the CV curves of MnO_2/SWNH/SWNT thin film electrodes in 0.1 M Na_2SO_4 as a function of dipping time at a scan rate of 50 mV/s. The potential window for cycling is confined between 0 and 0.8 V versus saturated calomel electrode (SCE) to avoid the oxygen evolution reaction at higher potential and MnO_2 dissolution at lower potentials.[18] The CV profiles exhibit nearly symmetrical rectangular shapes in potential window, which are ideal capacitive behaviors involving two types of capacitive contributing from electric double-layer capacitance

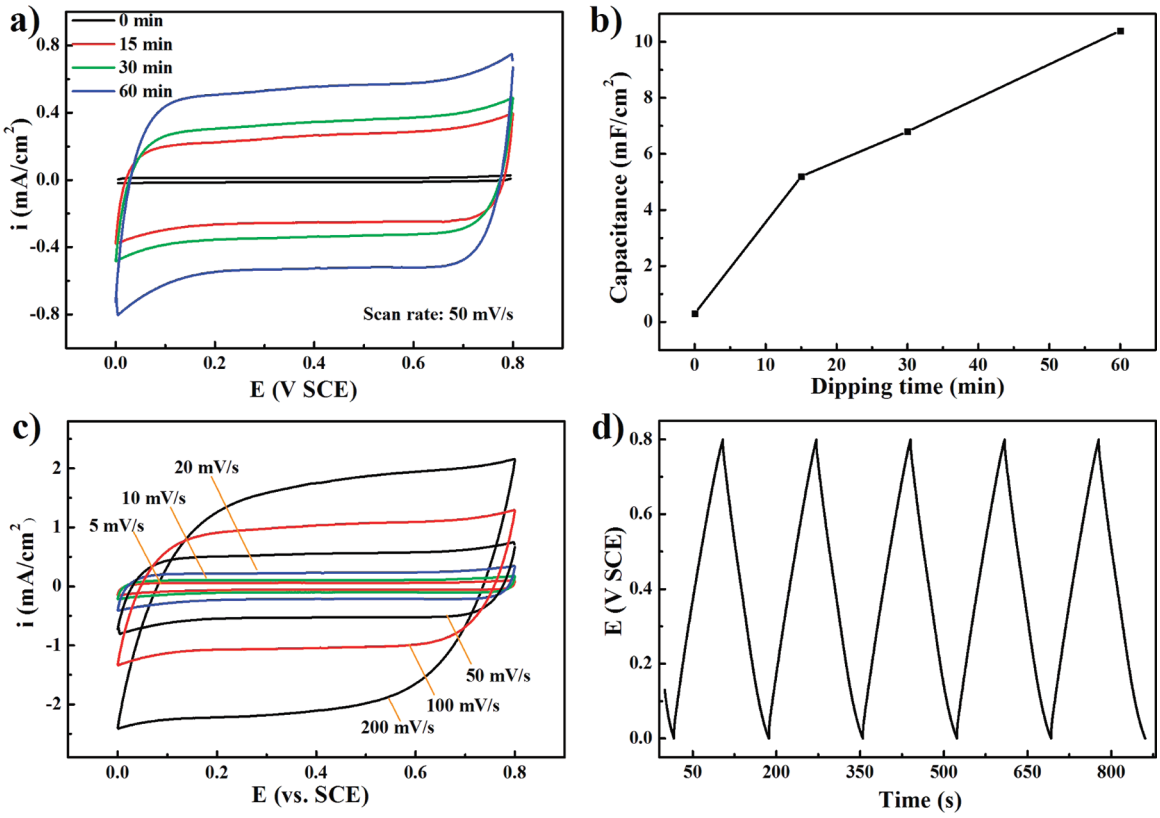

Figure 3. (a) Cycle voltammograms for MnO_2/SWNH/SWNT thin film electrodes in 0.1 M Na_2SO_4 as a function of dipping time. A scan rate of 50 mV/s was used; 0 min indicates a pristine SWNH/SWNT thin film. (b) Areal capacitance as a function of dipping time. Capacitance was estimated from cyclic voltammograms with a scan rate of 50 mV/s. (c) Cyclic voltammgorams for the trenary nanocomposites electrode (60 min dipping) at scan rates from 5 to 200 mV/s. (d) Galvanostatic charge−discharge curves of the ternary nanocomposites electrode (60 min dipping) at constant current density 3 A/g.

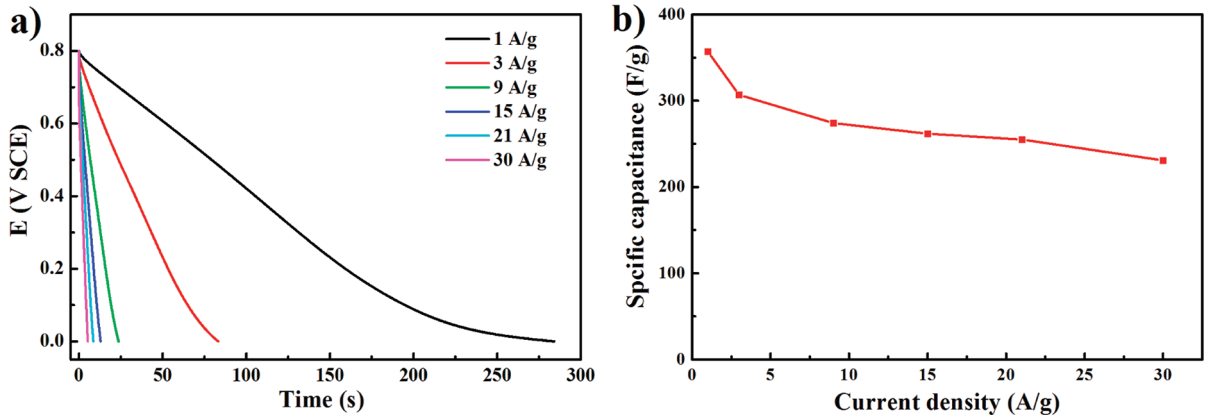

Figure 4. (a) Discharge curves and (b) specific capacitances of the MnO_2/SWNH/SWNT thin film nanocomposites electrode (60 min dipping) at different densities.

(EDLC) generated from SWNH/SWNT and pseudocapacitance from MnO_2.[6,14] The ideal capacitive behaviors are attributed to the structure of the ternary film electrodes. The SWNH/SWNT thin film electrode (0 min in Figure 3a) shows a current density of ~0.02 mA/cm^2 based on EDLC, indicating a lower capacitance in neutral aqueous electrolyte than in other medium.[19,20] Due to increasing of pseudocapacitive MnO_2, the current density strikingly rises for the ternary nanocomposite electrode. Also, the current densities increase with the dipping time, which results in increasing areal capacitances with dipping time (Figure 3b). At the same dipping time, the thin film electrode with the adding of SWNH shows higher capacitance comparing with the comparison of MnO_2/SWNT thin film electrode (see Figure S2 and Table S1 in the Supporting Information). Figure 3c shows the CV curves of the ternary nanocomposites electrode (60 min dipping) at scan rates over the range of 5−200 mV/s with potential windows ranging from 0 to 0.8 V versus SCE in 0.1 M Na_2SO_4 aqueous solution. These

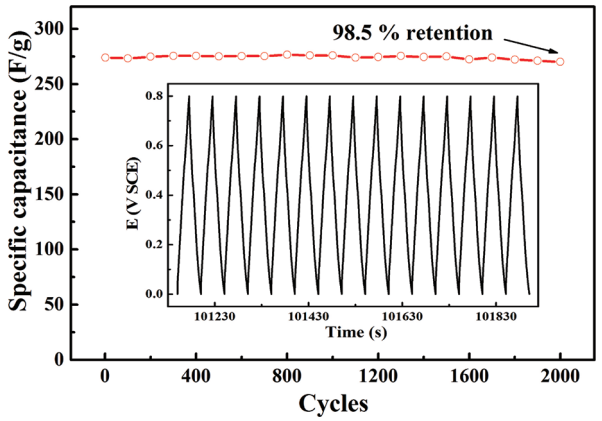

Figure 5. Cycling performance of MnO_2/SWNH/SWNT thin film electrode (60 min dipping). The inset shows the charge−discharge curves of the last 15 cycles.

CV curves show increasing densities with the scan rates and nearly rectangular shapes, indicating the fast charging/discharging process characteristic. Generally, the slow diffusion of ions in the electrode will lead to a nonideal rectangular shape of CV curve at a high scan rate. In this work, the porous structure of the MnO_2/SWNH/SWNT thin film electrode can shorten the diffusion path of the ions in the electrode. Hence, the curve still retains a rectangular shape even at a high scan rate of 200 mV/s, indicating the electrodes have ideal capacitive behavior and high-rate performance. Figure 3d shows the galvanostatic charge/discharge curve of ternary nanocomposites electrode (60 min dipping) at a current density of 3 A/g. The charging curves are near straight and very symmetric with the corresponding discharge counterparts, which also indicate a good electrochemical capacitive characteristic with the coulomb efficiencies closing to 100%. This result is corresponding to the CV testing. In addition, Figure 3d demonstrates the very stable charge−discharge cycles, as will be discussed later.

For further evaluating the rate capability of the MnO_2/SWNH/SWNT thin film electrode (60 min dipping), we carried out galvanostatic charge/discharge testing at different current densities. Current density is an important factor influencing the power behavior of supercapacitor. The discharge curves of ternary nanocomposites electrode at different current densities are shown in Figure 4a. There are low voltage losses even the current density increasing to 9 A/g, exhibiting low internal resistances within electrode for the directly coating of MnO_2 onto carbon matrix and the porous structure of ternary nanocomposites electrode. The specific capacitances of the electrode can be calculated according to the following formula: $C = I\Delta t/m\Delta V$, where I (A), Δt (s), m (g), and ΔV (V) are the discharge current, discharge time consumed in the potential range of ΔV, mass of the total electrode materials, and the voltage drop upon discharging (excluding the voltage loss), respectively.[21] The calculated specific capacitance is 357 F/g for the ternary nanocomposites electrode at a current density of 1 A/g. The corresponding specific capacitance based on MnO_2 is calculated according to formula: $C_{MnO2} = (Q_{MnO2/SWNH//SWNT} - Q_{SWNH/SWNT})/(\Delta V m_{MnO2})$, where $Q_{MnO2/SWNH/SWNT}$ and $Q_{SWNH/SWNT}$ are the voltammetric charge of the MnO_2/SWNH/SWNT and the SWNH/SWNT electrodes, ΔV and m_{MnO2} are the width of the potential window and the mass of MnO_2, respectively.[22] The value is 1190 F/g, approaching the theoretical value of MnO_2 (1370 F/g). The high specific capacitance value confirms that such design and fabrication of the MnO_2/SWNH/SWNT thin film electrode allow maximizing the utilization of MnO_2 pseudocapacity. The variation in specific capacitances of ternary nanocomposites electrode with an increasing current density are shown in Figure 4b. The ternary nanocomposites electrode can maintain a high specific capacitance well at high current density. As shown in Figure 4b, the ternary nanocomposites electrode preserves 65% of its initial specific capacitance (from 357 to 231 F/g) as the current density increasing from 1 to 30 A/g. Such superior rate capability can be attributed to the reduced diffusion path of ions, good access to electrolyte ions and high electrical conductivity based on the attractive porous structure of ternary nanocomposites electrode.

The cycle performances are of great importance for supercapacitors. The long cycling life test over 2000 cycles of the MnO_2/SWNH/SWNT thin film electrode (60 min dipping) was carried out at 9 A/g and the specific capacitance as a function of cycle numbers were presented in Figure 5. The curves demonstrate a stable ternary nanocomposites electrode with only less than 2% decay in available specific capacitance after 2000 cycles. The specific capacitance shows a slight increase due to the activation effect at the beginning of electrochemical cycling. The inset in Figure 5 shows the last 15 cycles of the ternary electrode, which shows a high coulomb efficiency and very stable charge−discharge cycles. It further demonstrates the ternary nanocomposites electrode is of a good long-term electrochemical stability. This result highlights the structure of ternary nanocomposites electrode to meet the requirement of long cycle lifetime, which is an important merit for practical energy storage devices.

Each component of the ternary nanocomposites electrode plays its unique role: SWNTs are the basic scaffold providing good conductivity, mechanical stability and high surface area for the ternary nanocomposites electrode. For its entangled feature, the binders are not needed for the preparation process of the thin films; SWNHs act key role of tuning the pore structure of the electrode, facilitating the rapid transport of the electrolyte ions and increasing the electrochemical utilization of MnO_2 pseudocapacity; The MnO_2 layer was directly coated on carbon matrix, providing the main pseudocapacitance and enabling the fast electron transfer within electrode. More important is that the components are not independent. The synergetic contribution from the components achieves a promising electrode with porous structure, high conductivity and good mechanical stability. These features allow a higher rate of electrolyte infiltration, facilitate the ions insertion/extraction and electrons transport in the electrode and thus decrease the ion diffusion path and electron transport resistance. Contributing from all these factors, the ternary nanocomposites electrode exhibits an attractive electrochemical performance.

In summary, a ternary thin film electrode of MnO_2/SWNH/SWNT was prepared by a facile method. The results of SEM and TEM exhibited it had an attractive porous structure, which ensured the fast redox reaction kinetics and easy electrolyte access to a large volume of active electrode materials. These factors enhance the charge transfer rate and total specific capacitance. The ternary nanocomposites electrode shows a specific capacitance of 357 F/g, and the value reaches up to 1190 F/g based on MnO_2. Also, the ternary nanocomposites electrode shows an excellent rate capability with specific capacitance preserved 65% with current density increasing from 1 to 30 A/g and good cycling performance of 98.5% retention after 2000 cycles. The ternary nanocomposites electrode

with an attractive structure is very promising for next-generation high-performance supercapacitors.

■ ASSOCIATED CONTENT

Supporting Information. Experimental details, characterization, specific surface area, and pore characterization of SWNT and SWNH/SWNT (Figure S1), CV tests for the comparisons (Figure S2, Table S1). This material is available free of charge via the Internet at http://pubs.acs.org.

■ AUTHOR INFORMATION

Corresponding Author
*Tel: 86-591-837928351. E-mail: guanlh@fjirsm.ac.cn.

■ ACKNOWLEDGMENT

Financial support for this study was provided by Chinese Academy of Sciences, and the National Key Project on Basic Research (Grant 2011CB935904), and the Natural Science Foundation of Fujian Province (Grant 2009J01044, 2010J05041).

■ REFERENCES

(1) Zhao, X.; Sánchez, B. M.; Dobson, P. J.; Grant, P. S. *Nanoscale* **2011**.
(2) Simon, P.; Gogotsi, Y. *Nat. Mater.* **2008**, *7*, 845.
(3) Zhang, L. L.; Zhao, X. S. *Chem Soc Rev* **2009**, *38*, 2520.
(4) Park, B.-O.; Lokhande, C. D.; Park, H.-S.; Jung, K.-D.; Joo, O.-S. *J Power Sources* **2004**, *134*, 148.
(5) Chunsheng, D.; et al. *Nanotechnology* **2005**, *16*, 350.
(6) Pan, H.; Li, J. Y.; Feng, Y. P. *Nanoscale Res. Lett.* **2010**, *5*, 654.
(7) Chen, J. H.; Li, W. Z.; Wang, D. Z.; Yang, S. X.; Wen, J. G.; Ren, Z. F. *Carbon* **2002**, *40*, 1193.
(8) Lee, S. W.; Kim, B.-S.; Chen, S.; Shao-Horn, Y.; Hammond, P. T. *J. Am. Chem. Soc.* **2008**, *131*, 671.
(9) Niu, Z.; Zhou, W.; Chen, J.; Feng, G.; Li, H.; Ma, W.; Li, J.; Dong, H.; Ren, Y.; Zhao, D.; Xie, S. *Energy Environ. Sci.* **2011**, *4*, 1440.
(10) Izadi-Najafabadi, A.; Yamada, T.; Futaba, D. N.; Yudasaka, M.; Takagi, H.; Hatori, H.; Iijima, S.; Hata, K. *ACS Nano* **2011**, *5*, 811.
(11) Lu, W.; Hartman, R.; Qu, L.; Dai, L. *J. Phys. Chem. Lett.* **2011**, 655.
(12) Lee, S. W.; Kim, J.; Chen, S.; Hammond, P. T.; Shao-Horn, Y. *ACS Nano* **2010**, *4*, 3889.
(13) Lota, K.; Sierczynska, A.; Lota, G. *Int. J. Electrochem.* **2011**, *2011*, 1.
(14) Wei, W.; Cui, X.; Chen, W.; Ivey, D. G. *Chem. Soc. Rev.* **2011**, *40*, 1697.
(15) Huang, X.; Yue, H.; Attia, A.; Yang, Y. *J. Electrochem. Soc.* **2007**, *154*, A26.
(16) Wu, C.; Guan, L. *Carbon* **2011**, *49*, 3267.
(17) Ge, J.; Qu, J. *Appl. Catal., B* **2004**, *47*, 133.
(18) Brousse, T.; Taberna, P.-L.; Crosnier, O.; Dugas, R.; Guillemet, P.; Scudeller, Y.; Zhou, Y.; Favier, F.; Bélanger, D.; Simon, P. *J Power Sources* **2007**, *173*, 633.
(19) Subramanian, V.; Zhu, H. W.; Wei, B. Q. *Electrochem. Commun.* **2006**, *8*, 827.
(20) Xie, X.; Gao, L. *Carbon* **2007**, *45*, 2365.
(21) Liu, J.; Jiang, J.; Cheng, C.; Li, H.; Zhang, J.; Gong, H.; Fan, H. J. *Adv. Mater.* **2011**, *23*, 2076.
(22) Lang, X.; Hirata, A.; Fujita, T.; Chen, M. *Nat Nano* **2011**, *6*, 232.